American Journal of Materials Engineering and Technology, 2017, Vol. 5, No. 1, 14-23
Available online at http://pubs.sciepub.com/materials/5/1/3
©Science and Education Publishing
DOI:10.12691/materials-5-1-3

On the Role of Boride in the Structural Integrity of a Turbine Disc Superalloy's Solid State Weld

K.M. Oluwasegun[1,*], J.O Olawale[1], M.D. Shittu[1], O.O. Ige[1], P.O. Atanda[1], O.O. Ajide[2], L.O. Osoba[3]

[1]Department of Materials Science and Engineering, Obafemi Awolowo University, Ile-Ife, Nigeria
[2]Department of Mechanical Engineering, University of Ibadan, Nigeria
[3]Department of Metallurgical and Materials Engineering, University of Lagos, Nigeria
*Corresponding author: excetom@gmail.com

Abstract This work reports the melting of boride precipitates along the grain boundary of a supposedly solid state welding of a polycrystalline superalloy, and discusses its attendant effect on the hot ductility behaviour of the alloy. Nickel-based superalloy used for this study was previously processed by hot extrusion of argon atomized powered followed by forging. The alloy was solution heat treated at 1120°C, aged at 760°C and subsequently air cooled to room temperature. Thereafter, it was welded by inertial friction welding (IFW) at a forging pressure of 250 MPa and finally stressed relieved at 760°C for 8 hours. The microstructures of welded samples were studied by scanning and scanning transmission electron microscopes. Gleeble hot ductility test was carried out on tensile specimen machined from the welded sample. The microstructures of the welded alloy shows that boride precipitates liquated along the grain boundary within the heat affected zone (HAZ) as a result of rapid heating of IFW. The results of hot ductility test revealed that the melting of boride lowered the hot ductility of the alloy. It was concluded that the boride precipitates liquated along the grain boundary of the nickel-based superalloy during solid state welding and lowered its hot ductility.

Keywords: *superalloy, solid state welding, boride precipitates, grain boundary, hot ductility, welding*

Cite This Article: K.M. Oluwasegun, J.O Olawale, M.D. Shittu, O.O. Ige, P.O. Atanda, O.O. Ajide, and L.O. Osoba, "On the Role of Boride in the Structural Integrity of a Turbine Disc Superalloy's Solid State Weld." *American Journal of Materials Engineering and Technology*, vol. 5, no. 1 (2017): 14-23. doi: 10.12691/materials-5-1-3.

1. Introduction

The need for more heat resistant materials in aircraft engine turbo superchargers prompted the development of superalloys in 1930s. It has been driven since the early 1940s by the increasing demands of advancing gas turbine engine technology [1]. In addition to aircraft applications, superalloys are now used in space vehicles, rocket engines, nuclear reactors, submarines, steam power plants, petrochemical equipment and other high-temperature applications. The largest use of superalloys, however, is the gas turbine industry [1]. The recent global demand in the reduction of emissions is also pertinent to aerospace industry. Achieving this goal of reducing emission by aerospace industry and consequently lowering its burden on the environment significantly requires a generation of jet engines that will burn fuel more effectively at higher temperature [1]. This stems the need for the development of new superalloys that offer heat resistance of which nickel base superalloys are candidate superalloys. Nickel-based superalloys among others have emerged as the choice for high-temperature application because of their FCC crystal structure, which confers good toughness and ductility, due to a considerable cohesive energy arising from the bonding provided by the outer d electrons [2]. This crystal structure is stable from room temperature to the melting point, so that there are no phase transformations leading to expansion and contraction, which might complicate its use for high temperature components. Their low rate of thermally activated processes (e.g. creep) and moderate cost have also contributed to their choice as candidate materials for high temperature applications. The high corrosion resistance observed in these alloys stems from the high level of chromium, as chromium forms an oxide layer which protects the material from further oxidation.

Addition of boron to nickel-base superalloys has been proposed to influence the chemistry and structure of the grain boundary precipitates [3]. It is generally known that the solid solubility of boron in austenitic γ alloys is very low [4]. For example, it was reported that the solubility of boron in 18%Cr-15%Ni stainless steel was 97 ppm at 1125°C. This solubility decreased rapidly with decreasing temperature, becoming less than 30 ppm at 900°C [25]. In addition to this, boron atoms are larger than the common interstitial elements (e.g carbon) but smaller than substitutional elements like Co and Cr. This misfit in size of boron atoms for substitutional and interstitial sites in austenitic lattices suggests that it could be energetically favorable for boron atoms to segregate to loosely packed regions like grain boundaries and incoherent interphase boundaries [5,6]. Kurban *et al* [7] have been able to report recently from their ion mass spectroscopy study of boron segregation that boron tends to have a stronger affinity for

partitioning into second phase particles than for remaining in solid solution on grain boundaries [7]. Borides are hard refractory particles observed only at grain boundaries. They are formed by the reaction of boron with elements like Cr, Mo and Ti. They vary in shape from blocky to half-moon or spherical in appearance. This reduces the onset of grain boundary tearing under rupture loading [1].

Complex-shaped components of superalloys are required with suitable elevated temperature mechanical properties and good hot corrosion resistance in order to withstand the stringent operating conditions encountered in the hot sections. Unfortunately, cost efficient commercial application of these materials has been largely restricted due to the difficulty in joining them by conventional welding techniques during manufacture and repair. This is because γ' precipitation hardened nickel-base superalloys are highly susceptible to heat affected zone (HAZ) microfissuring during welding and subsequent post weld heat treatments [8-16]. This connotes that as new and improved materials are developed to meet the severe high temperature environment challenge, then the challenge of welding them becomes even more demanding. To meet this welding challenge of new generation of high performance and high temperature superalloys, friction based solid state welding techniques are fast becoming industrial method of choice [17]. Inertia friction welding (IFW), a nominal solid state welding process that has existed for some time has now been employed in joining aero engine components since it does not involve any melting, provided that optimum welding parameters are chosen [17].

Grain boundary strengthening by the precipitation of borides is one of the strengthening mechanisms that have been employed for polycrystalline superalloys. Solid state welding of these alloys have been reported to proffer better high temperature mechanical properties than the conventionally fusion welding techniques based on the premise that melting is not involved [17]. However, the behaviour of the boride precipitates during solid state welding of polycrystalline superalloys has not been duly studied. Hence, this study.

2. Materials and Method

The material used in this work is a nickel-base superalloy, which was processed by hot extrusion of argon atomized powder and followed by forging. The parent alloy with chemical composition (wt%) 15.0Cr, 18.5Co, 5.0Mo, 3.0Al, 3.6Ti, 2.0Ta, 0.5Hf, 0.015B, 0.06Zr, 0.027C nickel balance, has been solution heat treated at 1120°C for 4 hours and aged at 760°C for 8 hours with subsequent air cooling, and it is applicable in turbine disc of aero or land based engine. The alloy was inertia friction welded at a forging pressure of 250 MPa, an upset of 5.4 mm and 0.79 mm/s linear burn off rate (LIBOR). It was thereafter subjected to a stress relieved post weld heat treatment (PWHT) at 760°C for 8 hours and air cooled. Gleeble hot ductility test was carried out by heating a tensile specimen to 1300°C at 20°C/s with an applied constant tensile load of 0.5 kN using a DSI Gleeble thermomechanical simulation system. Welded samples were sectioned parallel to the forging axis of the weld and the fractured hot ductility test samples were sectioned perpendicularly to the fracture surface. Both were prepared using standard metallographic procedures. An electrolytic etching using solution of water with a concentration of 10 % of orthophosphoric acid, at 3.5 V for 3 seconds was used to reveal the microstructure. This preferentially dissolves the γ phase leaving the γ' in relief. The microstructures were studied by an FEI-XL 30 field emission source scanning electron microscope and a JEOL 2100 scanning transmission electron microscope, each equipped with oxford instrument energy dispersive X-ray spectrometers with silicon drift detector (SDD). TEM samples were prepared by electropolishing technique using a Struers Tenupol-3 twin-jet electropolisher. The polishing was done in a solution containing 10% perchloric acid in 90% methanol at 20 V and -20°C to obtain transparency to the beam of electrons.

Thermodynamic simulation software (Thermo-Calc) along with assessed thermodynamic database TTNI7 was also used to study phase transformations in the multicomponent alloy. This is based on the computation, via complex thermodynamic descriptions of the various phases in a given system, of thermodynamic equilibria. A numerical minimization of the total Gibbs free energy of the alloy is performed at a given temperature by finding the optimal partition of elements into different phases and the optimal amounts of such phases [18]. This makes it possible to determine the amounts and compositions of the constituting phases as a function of temperature for a material of a given composition.

3. Results and Discussion

Figure 1a shows an SEM image of the parent alloy's microstructure, showing γ' precipitates and spherical borides. Representative image J output for area fraction quantification of the borides is presented in Figure 1b. Figure 1c is a TEM BF image of a typical boride in the alloy and its TEM EDX spectrum (Figure 1d), illustrating a significant boron concentration in the phase. The strong Mo and Cr peaks are characteristic of M_3B_2 and M_5B_3 borides. A further step was taken by examining this phase by TEM SADPs taken along three zone axes (Figure 2). This shows that they are M_3B_2 boride with a body centred tetragonal (bct) crystal structure with lattice parameters a=5.72 Å and c=3.07 Å. These boride precipitates were observed along the grain boundaries and their size lay between 250 nm and 390 nm with ~0.5% area fraction (Figure 1a, b). Other precipitates like MC carbides and hafnium oxides were also observed in the parent alloy. Table 1 shows the result of the chemical analysis of the observed precipitates within the parent alloy. All analyses were carried out on a transmission electron microscopy equipped with silicon drift EDX detector (SDD).

Precipitates with sizes below 50 nm (tertiary γ') were analyzed by TEM EDX using carbon extraction replicas, while others were analyzed using conventional thin foil specimens. The values in the Table 1 represent the average value for 12 different particles analyzed for each of the precipitates. Figure 3 shows the phase fraction against temperature of different phases calculated by Thermo-Calc using the nominal chemical composition of

the alloy. This profile shows that the solvus temperature of γ' (labelled as 5) is approximately 1155°C, and has been confirmed experimentally. The thermo-calc result has also been used to predict the solvus temperature of M_3B_2 (labelled 6 on the Thermo-Calc profile) and MC carbide (labelled 3) as 1150°C and 1286°C respectively.

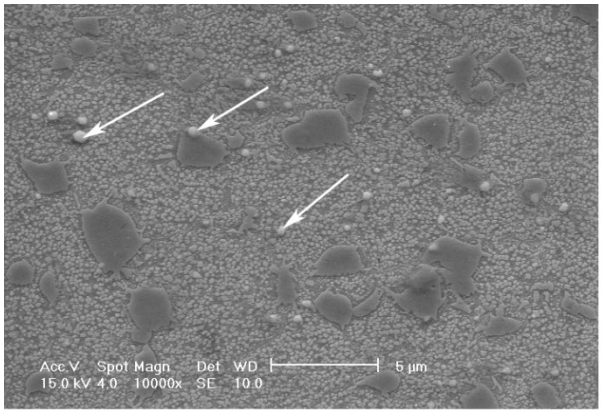

(A)

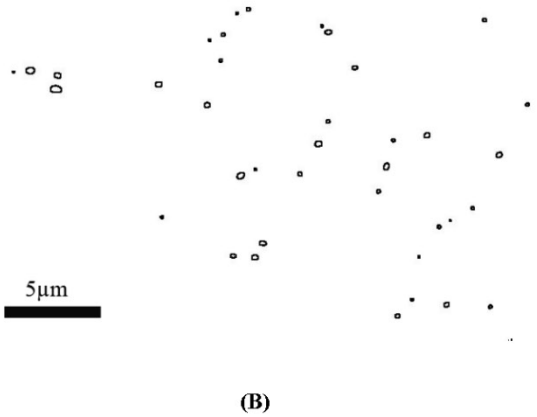

(B)

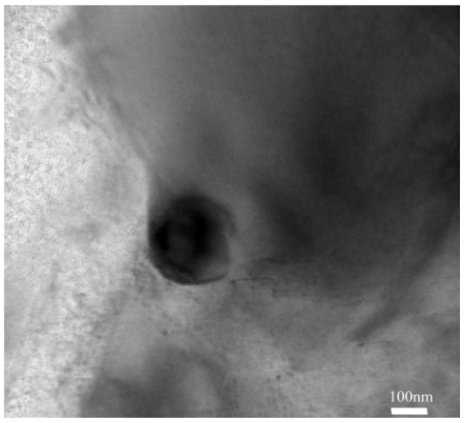

(C)

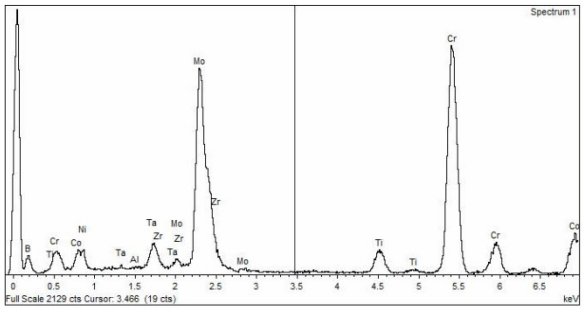

(D)

Figure 1. (a) SEM image of alloy 'X' showing γ' precipitates and grain boundary borides (insert arrows in 'a') (b) representative image J output for area fraction (%) quantification of boride in 'a' (c) TEM BF image of M_3B_2 boride (d) TEM EDX of M_3B_2 boride with strong Mo and Cr peaks.

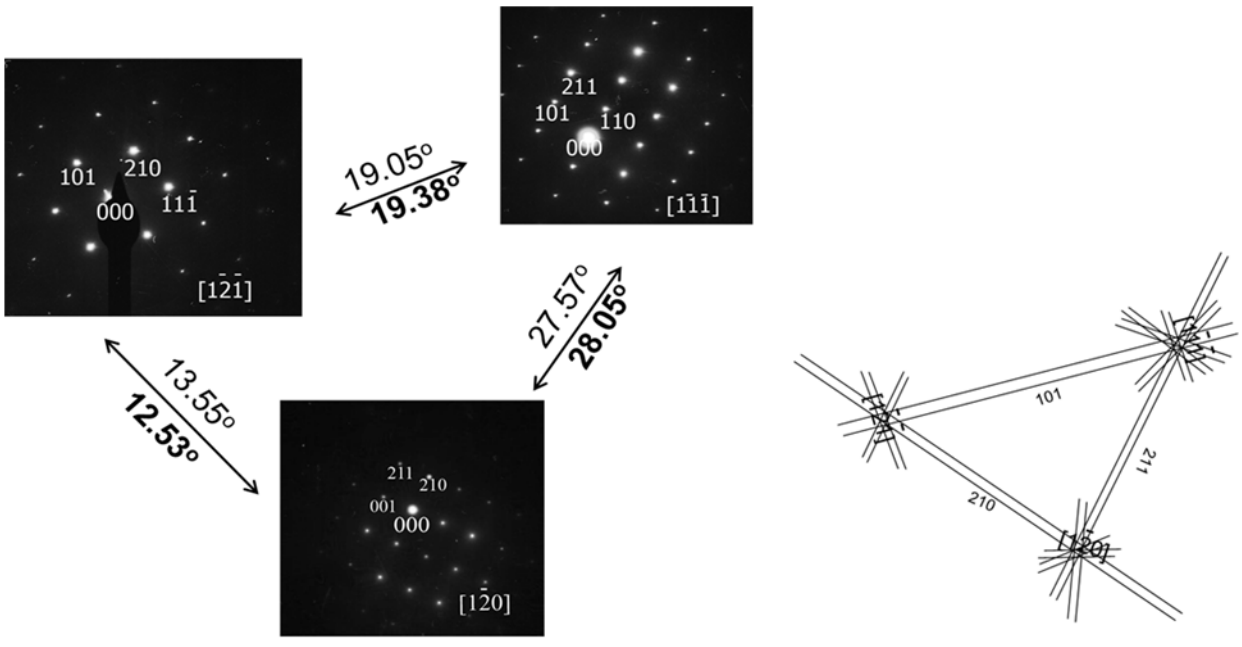

(A) (B)

Figure 2. SADPs taken from a boride particle along three zone axes; used to confirm the crystal structure (bct) and lattice parameter of the boride. (b) A schematic Kikuchi pattern along the three zone axes in 'a'.

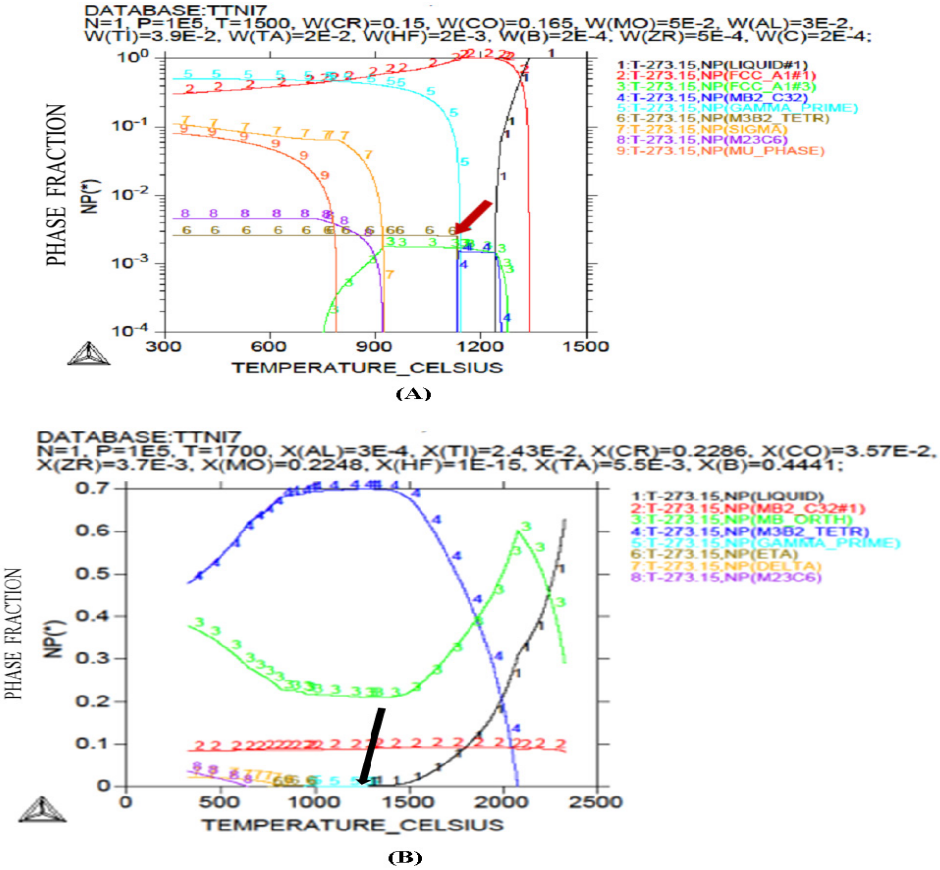

Figure 3. Thermo-Calc for (a) the nominal composition of the parent alloy, showing phase fraction vs temperature (Note that the predicted phases labelled 3, 6, 7, 8 and 9 were not observed in this work) (b) the composition of M_3B_2 boride. It predicts the onset of melting of the boride to be about 1200°C (insert black arrow)

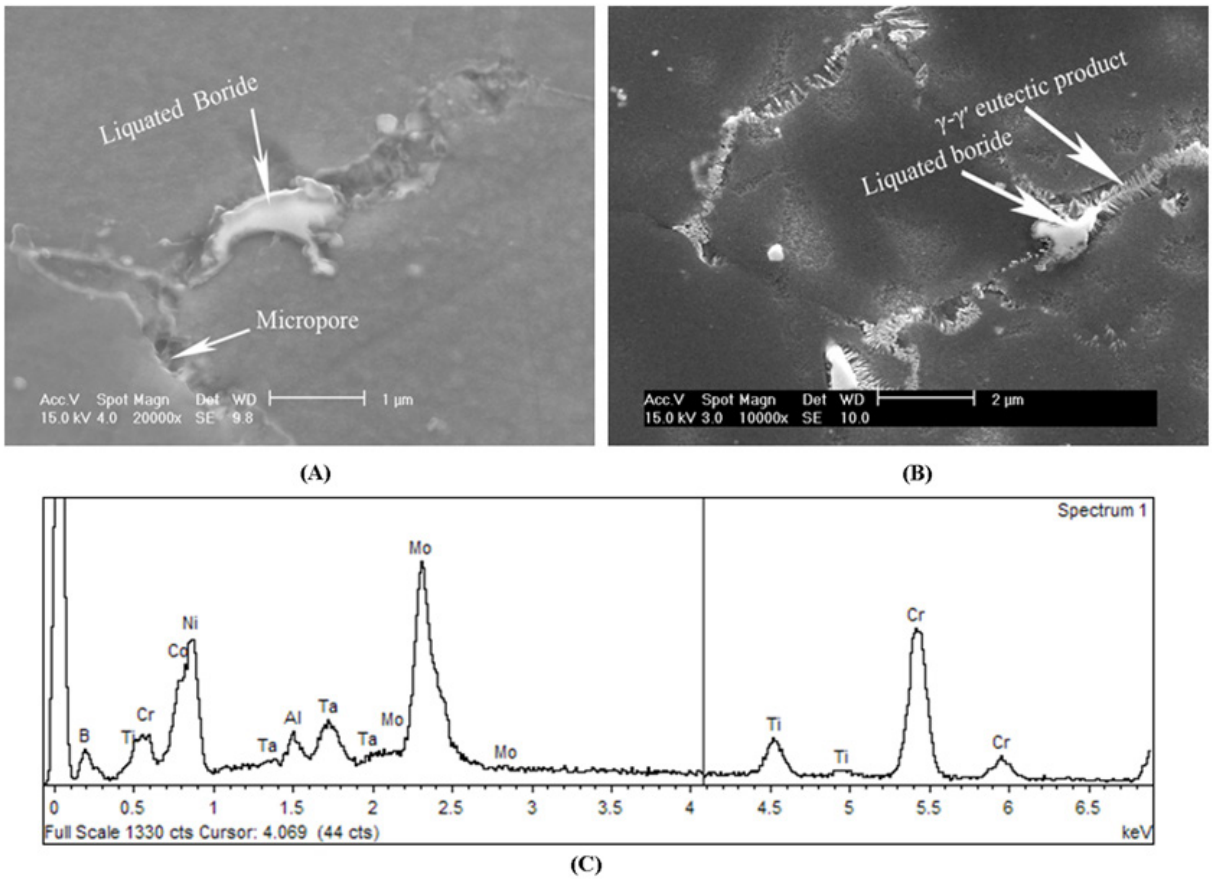

Figure 4. (a) SEM micrographs showing liquated boride along a grain boundary (GB) (b) a micrograph showing liquation products on the same GB from both boride and γ' precipitates (c) SEM EDX from the liquated boride

Table 1. Chemical Analysis of Precipitates in the Parent Alloy

Element (Atomic %)	Gamma Prime					
	Primary γ'	Secondary γ'	Tertiary γ'	MC	M_3B_2	HfO_2
AlK	10.14±1.1	13.53±0.4	13.69±0.32	0.0	0.0	0.72±0.14
TiK	9.24±0.6	8.12±0.7	8.01±0.62	24.09±1.2	2.19±0.6	0.61±0.17
CrK	4.22±1.4	1.59±0.43	1.41±0.81	3.06±0.4	22.35±0.4	1.43±0.32
CoK	11.54±0.51	7.53±0.52	6.59±1.4	2.21±0.3	3.99±0.2	1.25±0.21
NiK	62.01±1.8	65.42±1.32	67.74±2.14	5.38±0.3	3.18±0.3	7.51±1.03
ZrL	0.17±0.12	0.03±0.01	0.06±0.3	0.47±0.08	0.23±0.06	3.72±0.72
MoL	0.29±0.24	0.78±0.31	1.41±0.62	0.81±0.1	21.54±0.7	0.2±0.03
HfM	0.36±0.14	0.19±0.12	0.05±0.02	3.41±0.32	0.04±0.03	14.3±1.7
TaM	2.03±0.12	1.33±0.4	1.04±0.4	11.2±0.8	0.97±0.2	0.0
CK	0.0	0.0	0.0	49.4±1.4	0.0	0.0
BK	0.0	0.0	0.0	0.0	45.5±1.2	0.96±0.13
OK	0.0	0.0	0.0	0.0	0.0	69.30±2.03

3.1. Microstructure of the Welded Alloy

It has been extensively studied and reported that primary γ' precipitates constitutionally liquated within the heat affected zone of different nickel-based superalloys during different welding techniques [12,13,19,20], thus, that is not the focus of this paper. In this work, aside from the primary γ' precipitates that were observed to liquate constitutionally within the weld heat affected zone, the M_3B_2 precipitates found in the parent alloy have also been observed to liquate within the heat affected zone (150-360 μm from the weld bond line). Figure 4 a is an SEM micrograph showing liquated boride along a grain boundary. Concurrent liquation of boride and primary γ' along the same grain boundary was also observed (Figure 4 b). The SEM EDX spectrum (Figure 4c) shows B, Cr and Mo peaks which are the main elements in M_3B_2. The liquation of M_3B_2 within the heat affected zone is evident from morphological point of view

M_3B_2 in the parent material are spherical) and is also consistent with the Thermo-Calc results, showing that the melting of M_3B_2 could be initiated at about 1200°C. The solvus temperature of M_3B_2 (see composition in Table 1) predicted by Thermo-Calc for the nominal composition of the parent alloy is approximately 1150°C, (red arrow in Figure 3a) which is close to the solvus temperature of primary γ' (1155°C), and thus they could have survived the solvus temperature and melted by the rapid heat of welding at the thermodynamically favored temperature of welding. The maximum temperature reached by a typical inertia friction welding (similar to present work) of a polycrystalline superalloys has been modeled and described to be about 1200°C [21].

Further steps were taken to identify the crystal structure of the liquated boride. Figure 5a is a TEM BF image of a liquated boride along a decohesed grain boundary. STEM SDD mapping (Figure 5b) and quantitative results (Table 2) show this particle to be a Cr and Mo-rich boride. SADPs (Figure 6) taken from this liquated particle along two zone axes are consistent with a body centred tetragonal crystal structure with lattice parameters a = 5.70 Å and c = 3.04 Å, characteristic of M_3B_2.

Figure 7 shows that within the heat affected zone where primary γ' and M_3B_2 liquated, MC carbides were unaffected by the heat from the welding. Although the area fraction of MC carbide was less than 1%, they were still found pinning grain boundaries, and could therefore prevent significant grain growth in the region. Figure 8 shows another region of the heat affected zone where the melting of boride was associated with grain boundary decohesion. The EDX mapping clearly shows that the feature within the decohesed grain boundary is Cr-Mo and also shows the presence of boron, which is typical of boride in the superalloy understudy. An unaffected blocky Ti-Ta-rich MC carbide is also apparent close to the melted boride in Figure 8, which corroborates the observation in Figure 7.

3.2. Melting of M_3B_2 Boride within the HAZ

During rapid heating of IFW, where diffusion time is limited, dissolution of borides (solvus ~1200°C, refer to Figure 3) may be delayed until the temperature reaches a point where borides can thermodynamically melt (Figure 4, Figure 5, Figure 7 and Figure 8). Also, various investigators [22,23,24] have reported that the liquation of boride within the HAZ of fusion welded nickel-based alloys was due to insufficient time for homogenization by diffusion of boron during the rapid heating of welding, which resulted in considerable enrichment of grain boundary regions with boron (melting point depressant). According to B-Cr-Mo phase diagram for an M_2B type boride (Figure 9) [27], it is possible that enrichment of boron in a boride/matrix system can lower the solidus temperature and thus enhance the melting of the boride. It may be argued that the observed hole in the micrographs (Figure 5 and Figure 8) may not be directly linked to the occurrence of boride liquation in the alloy since it is possible for some precipitates (e.g MC carbide) to have fallen out from the site, but it is important to mention that this type of micro cavity has been observed in other boride liquated grain boundaries in the same weld. Thus, sufficient thermal stress/strain due to thermal gradient during welding could also be a possible cause of the observed voids due to the decohesion of the weak grain boundary where boride liquated.

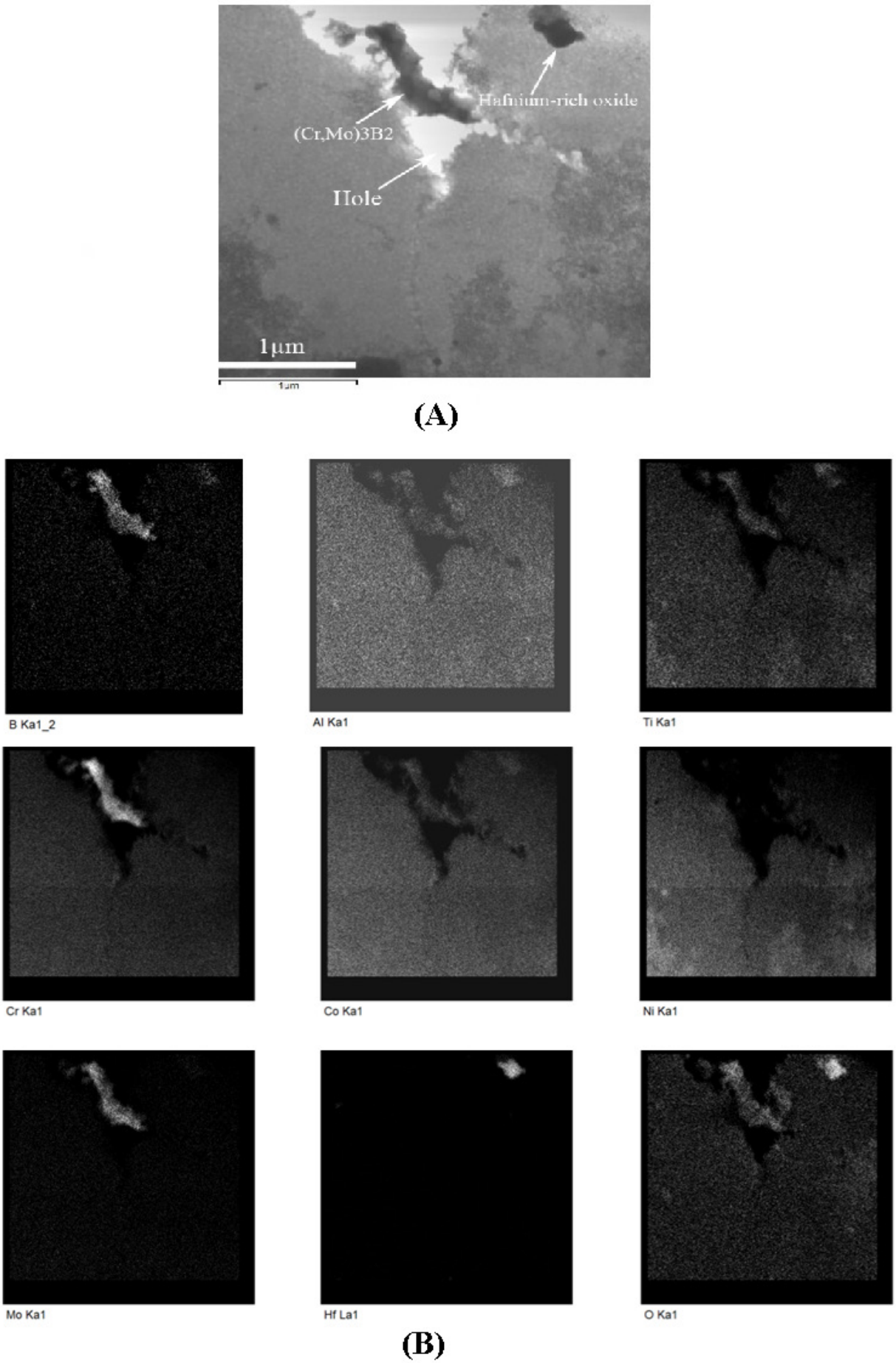

Figure 5. (a) STEM BF image of a liquated M_3B_2 particle and a Hf-rich oxide (b) STEM EDX maps of the liquated phase in 'a'.

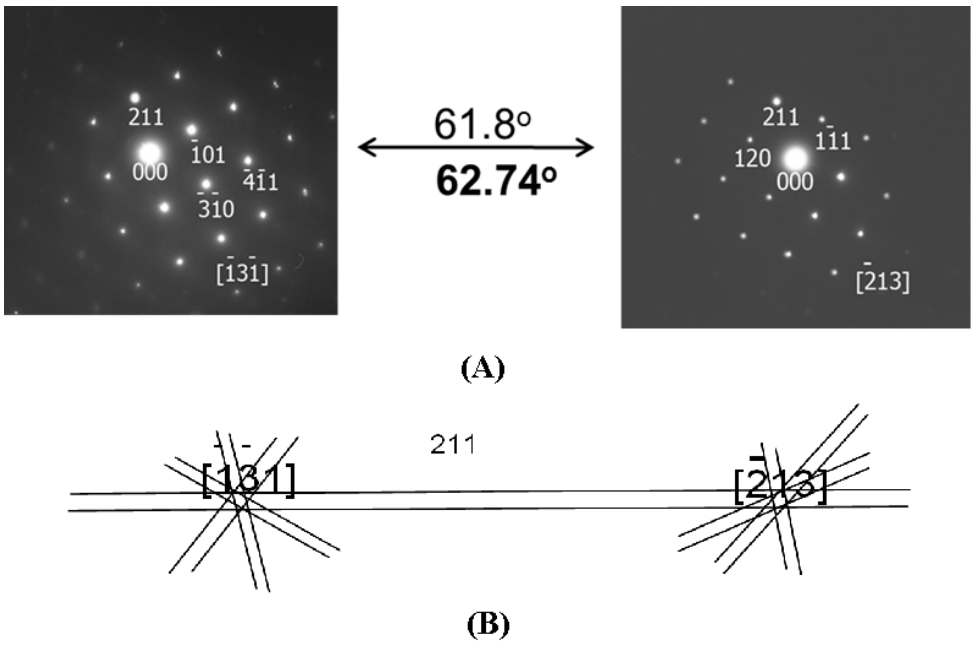

Figure 6. (a) SADP from the liquated boride shown in Figure 5. The bold angle is the total tilt angle while the unbold is the calculated angle. (b) Schematic Kikuchi pattern along the zones in 'a'

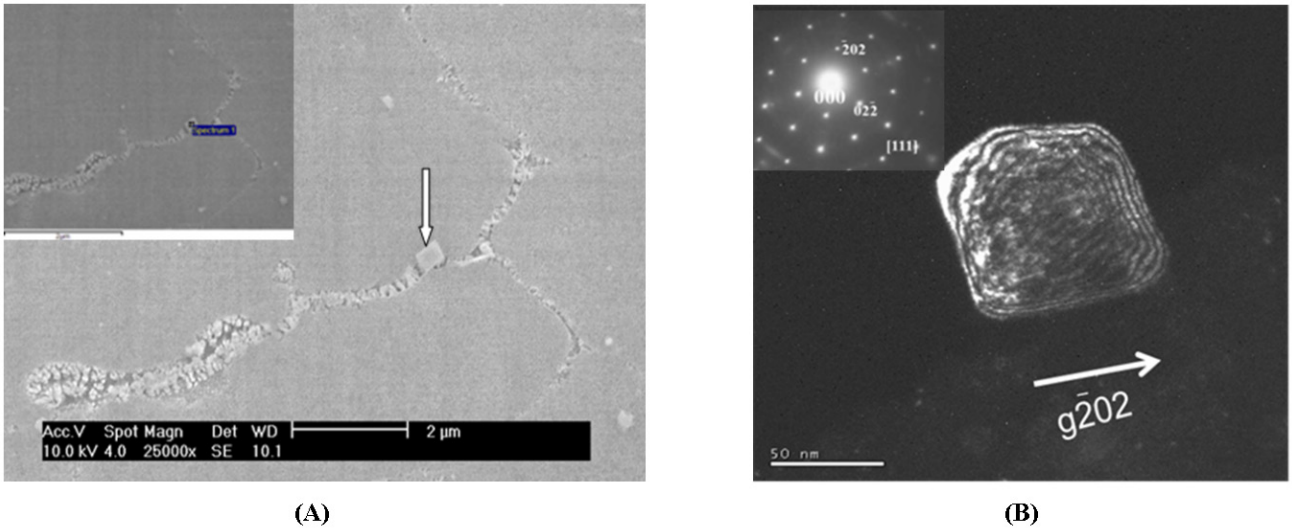

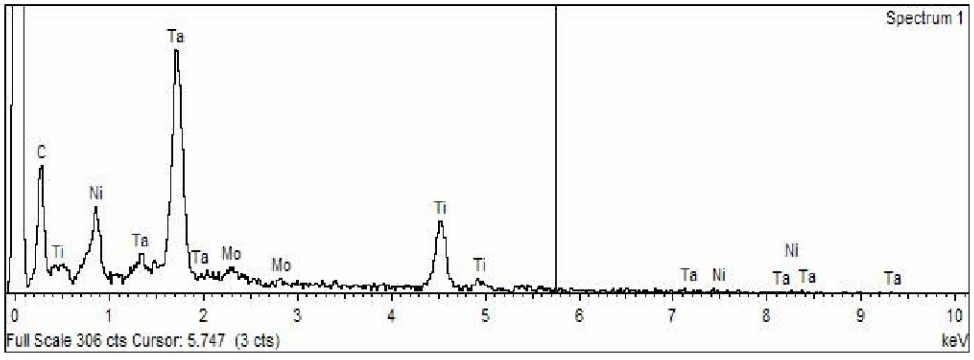

Figure 7. (a) SEM image of MC carbide within the CLZ (b) TEM DF image of a different intergranular MC carbide within the heat affected zone with insert SADP (c) SEM EDX spectrum of the MC carbide in 'a'. MC carbides in this region of the weld are clearly unaffected by the heat of welding.

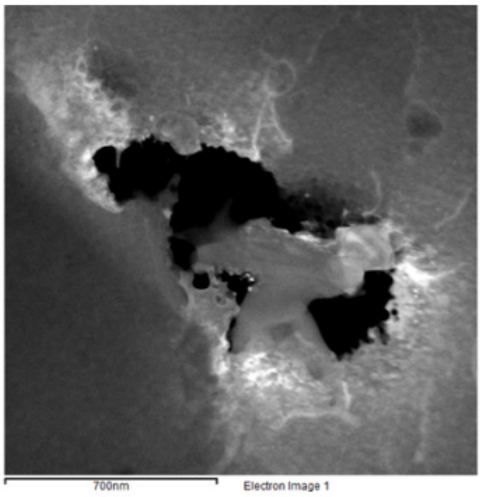

(A)

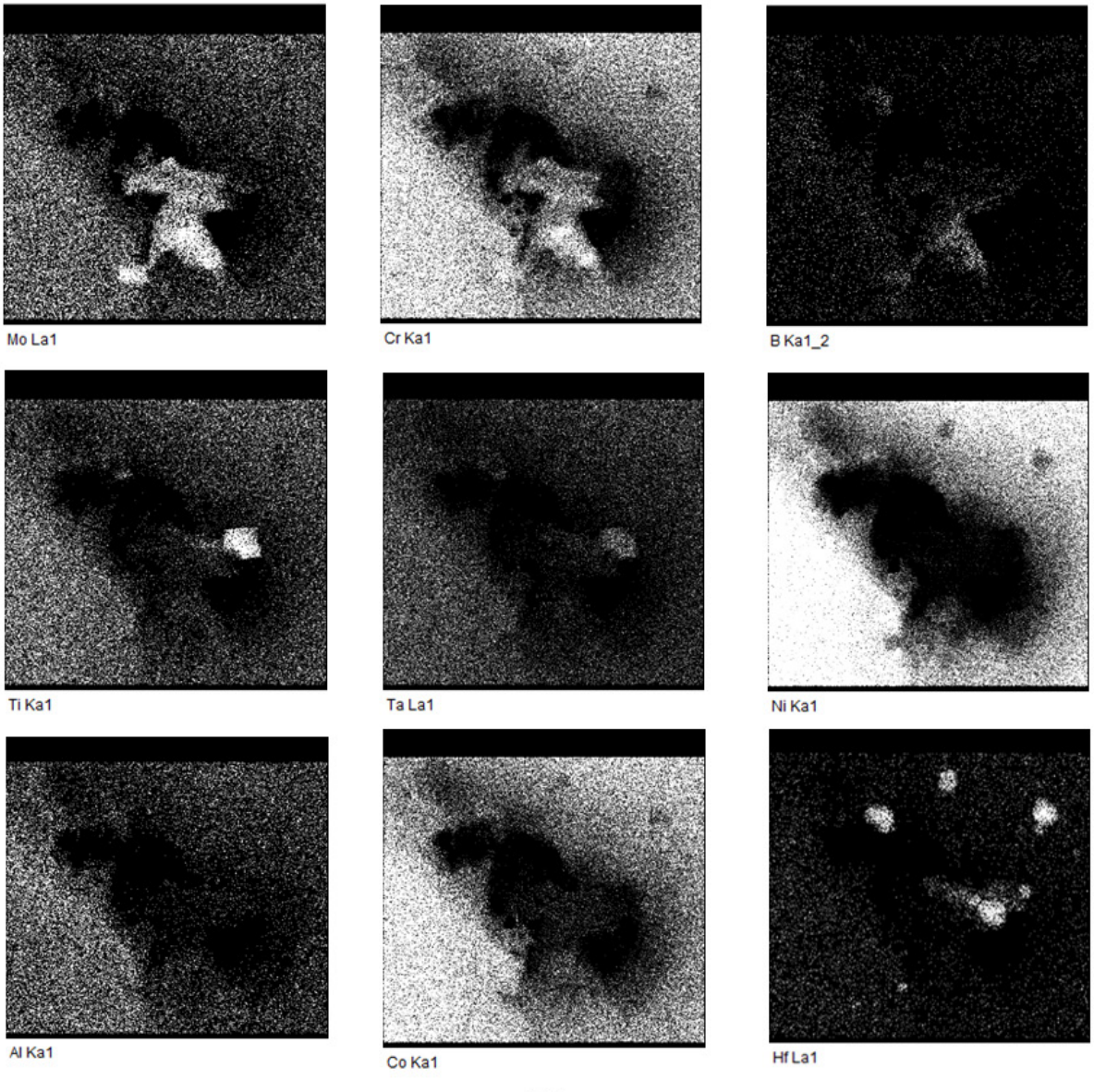

(B)

Figure 8. (a) STEM BF image of a liquated M_3B_2 particle associated with unaffected MC carbide and hafnium oxide (b) STEM EDX maps of the liquated phase in 'a'.

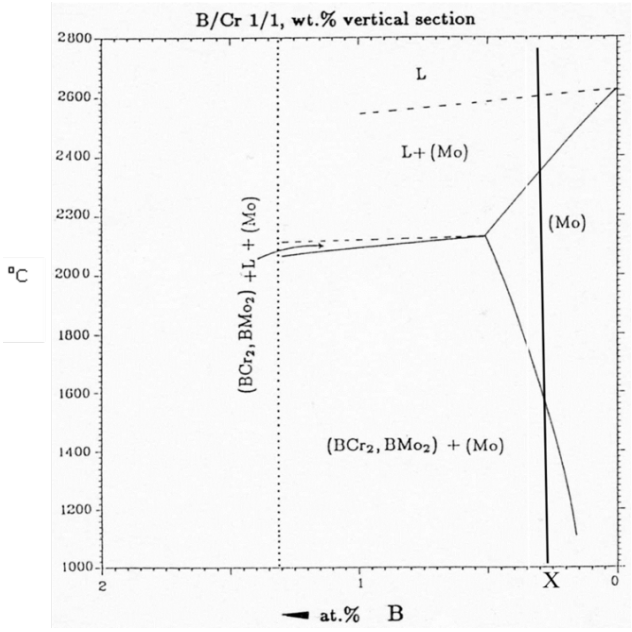

Figure 9. B-Cr-Mo phase diagram showing the effect of boron on increasing the melting temperature range of an M_2B boride [25]

3.3. Effect of Melting of Precipitates on the Hot Ductility of the Alloy

The susceptibility of structural alloys to weld HAZ microcracking is often quantified by Gleeble hot ductility testing [26,27]. Thus, in order to validate the effect of constitutional liquation of grain boundary precipitates within the HAZ of this alloy during inertia friction welding, Gleeble hot ductility testing has been employed in this work. This test is based on the premise that the deformation behavior of a material, as evaluated by its hot ductility, reflects its capability to accommodate tensile stresses and resist cracking during welding [27].

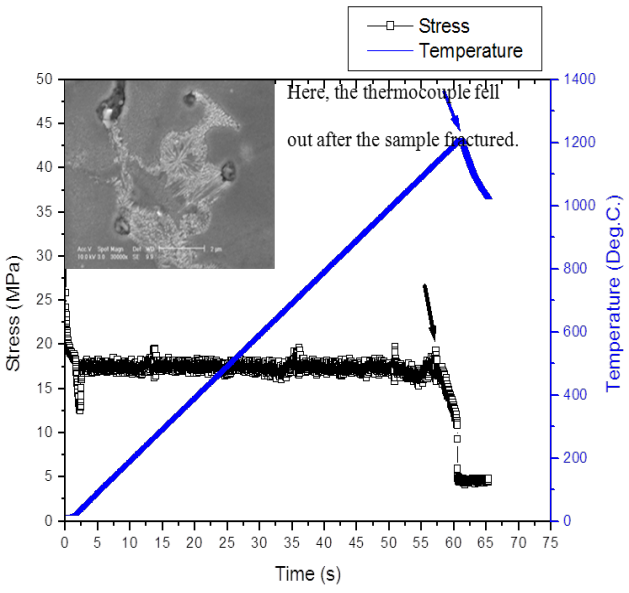

Figure 10. Stress and temperature profile during Gleeble on-heating ductility test of nickel-based superalloy with insert microstructure observed adjacent to the fractured surface. The arrows on the plot illustrate the correspondence between the temperature where liquation of the precipitates occurs and the abrupt drop in stress level

Figure 10 shows stress vs temperature profile of a Gleeble tensile specimen heated to 1300°C at 20°C/s with an applied constant tensile load of 0.5 kN. The sample failed during the test with an abrupt drop in the load at about 1214°C, which is below the solidus temperature of the alloy (1243°C) as predicted by Thermo Calc (Figure 3a).

The ductility measured after the material failed was zero (no change in the diameter of the failed sample). The temperature at which the material failed is consistent with the temperature where liquation of precipitates (both γ' and boride) occurred in the alloy as shown in this work. The microstructure adjacent to the fracture surface of the tested sample was examined, and liquation products of boride and γ' were found to decorate the grain boundary as shown in the insert of Figure 10. This observation illustrates that the strength of the alloy could be affected by the liquation of precipitates within heat affected zone during welding. The release and diffusion of boron, a known melting point depressant element by the melting of boride during the supposedly solid state welding of the superalloy could worsen the reduction of ductility within the region and thus the failure of the material.

4. Conclusion

Grain boundary strengthening boride precipitates have been observed to melt during a supposedly solid state welding process. This has the propensity of lowering the hot ductility property of the alloy during welding and consequentially enhancing decohesion of grain boundaries. The response of boride to very rapid heating of inertia friction welding in this work could be similar to other solid state welding techniques, where M_3B_2 borides strengthened polycrystalline superalloys are being welded, thus adequate attention is required.

Acknowledgement

The authors would like to acknowledge The School of Metallurgy and Materials of The University of Birmingham, United Kingdom for the access to the facilities needed to make this research a success.

References

[1] W.C. Hagel, The Superalloys, John Wiley & Sons, New York, 1972.

[2] R.C. Reed, The Superalloys, Fundermentals and Applications, University Press, Cambridge, 2006.

[3] A.F. Padilha, G. Schanz, Precipitation of a boride phase in 15-percent-Cr-15-percent-Ni-Mo-Ti-B austenitic stainless-steel (DIN 1.4970), Journal of Nuclear Materials 95 (1980) 229-238.

[4] C. Stocker, M. Zimmermann, H.J. Christ, Z.L. Zhan, C. Cornet, L.G. Zhao, M.C. Hardy, J. Tong, Microstructural characterisation and constitutive behaviour of alloy RR1000 under fatigue and creep-fatigue loading conditions, Material Science and Engineering A 518 (2009) 27-34.

[5] D.H. Maxwell, J.F. Baldwin, J.F. Radavich, New concept in superalloy ductility, Metallurgia and Metal Forming 42 (1975) 332.

[6] H.R. Zhang, O.A. Ojo, Cr-rich nanosize precipitates in a standard heat-treated Inconel 738 superalloy, Philosophical Magazine 90 (2010) 765-782.

[7] M. Kurban, U. Erb, K.T. Aust, A grain boundary characterization study of boron segregation and carbide precipitation in alloy 304 austenitic stainless steel, Scripta Materialia, 54 (2006) 1053-1058.

[8] W.A. Owczarski, D.S. Duvall, C.P. Sullivan, Model for heat-affected zone cracking in nickel-base superalloys, Welding Journal 45 (1966) 145-155.

[9] M. Prager, C.S. Shira, Welding of precipitation-hardening nickel-base alloys, Welding Research Council - Bulletin Series 128 (1968) 55.

[10] M.H. Haakens, J.H.G. Matthey, New approach to the weldability of nickel-base as-cast and powder metallurgy superalloys, Welding Journal 61 (1982) 25-30.

[11] T.J. Kelly, Welding metallurgy of investment cast nickel-based superalloys, Weldability of Materials 1990 151-157.

[12] O.A. Ojo, R.G. Ding, M.C. Chaturvedi, Heat affected zone microfissuring in a laser beam welded directionally solidified Ni_3Al-base alloy, Scripta Materialia 54 (2006) 2131-2136.

[13] G. Cam, M. Kocak, Progress in joining of advanced materials, International Materials Reviews 43 (1998) 1-44.

[14] M.B. Henderson, D. Arrell, M. Larsson, G. Marchant, Nickel based superalloy welding practices for industrial gas turbine applications, Science and Technology of Welding and Joining 9 (2004) 13-21.

[15] J.K. Tien, T.J. Caulfield, Superalloys, Supercomposites and Superceramics, Academic Press Inc, London, 1989.

[16] Z.W. Huang, H.Y.Li, M. Preuss, M. Karadge, P. Bowen, S. Bray, G. Baxter, Inertia friction welding dissimilar nickel-based superalloys alloy 720Li to IN718, Metallurgical and Materials Transactions A – Physical Metallurgy and Materials Science 38A (2007) 1608-1620.

[17] M. Preuss, J.W.L. Pang, P.J. Withers, G.J. Baxter, Inertia welding nickel-based superalloy: Part II. Residual stress characterization, Metallurgical and Materials Transactions A: Physical Metallurgy and Materials Science 33 (2002) 3227-3234.

[18] F. Tancret, Thermo-Calc and Dictra simulation of constitutional liquation of gamma prime (γ') during welding of Ni base superalloys, Computational Materials Science 41 (2007) 13-19.

[19] K.M. Oluwasegun, J.O. Olawale, O.O. Ige, M.D. Shittu, A.A. Adeleke, B.O. Malomo, Microstructural characterization of thermomechanical and heat-affected zones of an inertia friction welded astroloy, Journal of Materials Engineering and Performance 23 (2014) 2834-2846.

[20] R.K. Sidhu, O.A. Ojo, M.C. Chaturvedi, Microstructural analysis of laser-beam-welded directionally solidified Inconel 738, Metallurgical and Materials Transactions A: Physical Metallurgy and Materials Science 38 (2007) 858-870.

[21] L. Wang, M. Preuss, P.J. Withers, G. Baxter, P. Wilson, Energy-input-based finite-element process modeling of inertia welding, Metallurgical and Materials Transactions B: Process Metallurgy and Materials Processing Science 36 (2005) 513-523.

[22] H.A. Shahsavari, A.H. Kokabi, S. Nategh, Effect of preweld microstructure on HAZ liquation cracking of Rene 80 superalloy, Materials Science and Technology 23 (2007) 547-555.

[23] R.K. Sidhu, O.A. Ojo, M.C. Chaturvedi, Microstructural response of directionally solidified Rene 80 superalloy to gas-tungsten arc welding, Metallurgical and Materials Transactions A: Physical Metallurgy and Materials Science 40 (2009) 150-162.

[24] O.A. Ojo, N.L. Richards, M.C. Chaturvedi, Study of the fusion zone and heat affected zone microstructures in tungsten inert gas-welded INCONEL 738LC superalloy, Metallurgical and Materials Transactions A – Physical Metallurgy and Materials Science 37A (2006) 421-433.

[25] P. Villars, A. Prince, H.Okamoto, Handbook of Ternary Alloy Phase Diagram 5 (1995) 5526.

[26] O.A. Ojo, M.C. Chaturvedi, On the role of liquatedγ' precipitates in weld heat affected zone microfissuring of a nickel-based superalloy, Materials Science and Engineering A – Structural Materials Properties Microstructure and Processing 403 (2005). 77-86.

[27] W. Lin, J.C. Lippold, W.A. Baeslack, An evaluation of heat-affected zone liquation cracking susceptibility.1. Development of a method for quantification, Welding Journal 72 (1993) 135-153.